

Magnetic-field enhancement of the exciton-polariton splitting in a semiconductor quantum-well microcavity: The strong coupling threshold

J. D. Berger, O. Lyngnes, H. M. Gibbs, G. Khitrova, T. R. Nelson, and E. K. Lindmark
Optical Sciences Center, University of Arizona, Tucson, Arizona 85721

A. V. Kavokin and M. A. Kaliteevski
A. F. Ioffe Physico-Technical Institute, 26 Polytekhnicheskaya, St. Petersburg 194021, Russia

V. V. Zapasskii
St. Petersburg State University, Vavilov State Optical Institute, Petrodvorets, St. Petersburg, Russia
(Received 2 January 1996)

We investigate the influence of strong magnetic confinement on an exciton coupled to the resonant mode of a semiconductor microcavity. Cavity mode coupling to a variety of discrete exciton resonances is described in direct relation to the quantum-well magnetoabsorption spectra. We show that the magnetic-field-enhanced vacuum Rabi splitting and time-resolved oscillation frequency obey the predicted square-root dependence on the exciton oscillator strength computed directly from the integrated absorption spectra. Anticrossing curves measured in zero field and in 11.25 T evidence an interesting three-oscillator coupling observable only at high fields due to enhanced higher-order light-hole-exciton transitions. The data are in excellent agreement with a theoretical model which deduces magnetic-field-dependent oscillator strengths and corresponding reflectance spectra from a variational calculation combined with a transfer matrix method. [S0163-1829(96)03027-5]

I. INTRODUCTION

The strong coupling regime of cavity quantum electrodynamics^{1,2} is particularly interesting because it is in this regime that one can best take advantage of the coherent energy transfer between emitter and cavity modes to favor emission into the cavity mode over the other transversely propagating modes, leading to the possibility of an efficient light-emitting diode (LED) or very low threshold laser, for example.² To achieve the strong coupling regime, the emitter-cavity mode interaction must dominate over irreversible decay mechanisms due to spontaneous emission and cavity losses. In other words, the strong coupling regime is reached when $\Omega_0 \gg \kappa, \gamma$, where $\hbar\Omega_0$ is the vacuum Rabi splitting energy, κ is the cavity mode linewidth, and γ is the emitter spontaneous emission linewidth.³

The present paper investigates the strong coupling regime for a semiconductor microcavity under an applied magnetic field. Semiconductors in strong magnetic fields are known to exhibit enhanced dipole moments due to reduced dimensionality imposed by the magnetic confinement.⁴⁻⁶ It has recently been shown that a strong magnetic field applied to a semiconductor quantum-well microcavity increases the vacuum Rabi splitting, bringing Landau level transitions into the strong coupling regime.^{7,8} Here time-resolved reflectivity of the magnetoexciton-polariton system is used to demonstrate that an applied magnetic field leads to faster Rabi oscillations. Furthermore, a strong magnetic field enhances weakly allowed higher-order light-hole-exciton states so dramatically as to propel them into the strong coupling regime. The essential physics behind these observations, namely, magnetic-field enhancement of the exciton oscillator

strength, proportional to the square of the coupling strength, is confirmed by direct measurement of the relative oscillator strength from magnetoabsorption data, combined with vacuum Rabi splitting and time-resolved oscillation measurements.

A semiconductor, with its continuum of electronic states, may at first seem an imposing system for the observation of the vacuum Rabi splitting. We can, however, take advantage of the Coulomb interaction between electron-hole pairs which leads to discrete exciton bound states below the continuum band edge. Exciton polaritons, or coupled exciton-photon modes, are observed in bulk semiconductors when the exciton is brought into resonance with an electromagnetic field mode.⁹ To observe the vacuum Rabi splitting, the semiconductor must be placed in a cavity where the exciton is coupled to a single cavity mode. This can be done, in practice, in a semiconductor microcavity.^{10,11} The coupling strength may be increased even further by taking advantage of semiconductors with reduced dimensionality, which exhibit significant enhancement of excitonic absorption features due to the quantization of the electron envelope wave functions.¹² For this reason, a quantum well placed at the center of a semiconductor microcavity provides an ideal coupled system. Indeed, the first observations of the vacuum Rabi splitting in a quantum-well semiconductor microcavity^{10,11} and subsequent time-resolved Rabi oscillation measurements¹³⁻¹⁶ unleashed a wealth of possibilities for both fundamental and practical studies of quantum optics in semiconductors.

The vacuum Rabi splitting $\hbar\Omega_0$ is given by $2\phi E_0$, where ϕ is the dipole transition matrix element and $E_0 = \sqrt{\hbar\omega_c/2\epsilon V_c}$ is the electric field per photon, ω_c being the

cavity resonance frequency and V_c the cavity mode volume. For a single quantum well placed at the center of a λ microcavity, Ω_0 can be expressed as $\Omega_0 \cong [2c\Gamma_0 / \sqrt{\epsilon_c}(L_c + L_{\text{DBR}})]^{1/2}$,¹⁷ where Γ_0 is the exciton radiative damping rate, ϵ_c is the cavity spacer dielectric constant, L_c is the length of the central layer of the microcavity, and L_{DBR} is the characteristic length of the distributed Bragg reflectors. The exciton radiative damping rate can be written in terms of the oscillator strength per unit area per quantum well (f_e/A) as $\Gamma_0 = \pi e^2(f_e/A) \sqrt{\epsilon_c} mc$,¹⁷ where m is the free electron mass and the electromagnetic field dependence of the splitting is contained in f_e . Enhanced excitonic absorption will therefore increase the coupling strength between the exciton and the cavity mode. We note that the quantum well area A times the effective cavity length $L_c + L_{\text{DBR}}$ is an approximation to the true cavity mode volume V_c .

This strong enhancement can be taken one step further by combining vacuum Rabi coupling with the sharp excitonic features of a quasi-zero-dimensional semiconductor.^{7,8} We can create a quasi-zero-dimensional exciton within the semiconductor quantum-well microcavity by applying a perpendicular magnetic field. The magnetic field subjects the photon-generated electron-hole pairs to a transverse quadratic confining potential, which results in quantized magnetoexciton states. These states appear in the linear absorption spectrum as a series of isolated peaks, which are characteristic of a quasi-zero-dimensional system.⁴⁻⁶ The magnetic-field strength controls the magnetoexciton radius, and so by increasing the field, it is possible to study the transition from a quasi-two-dimensional to a quasi-zero-dimensional magnetoexciton. Under strong magnetic field, the exciton undergoes a diamagnetic shift to higher energies accompanied by an increase in the exciton oscillator strength due to wavefunction shrinkage.¹⁸⁻²⁰ This increase in oscillator strength results in substantial enhancement of the magnetoexciton-polariton splitting.

In this paper, we present an experimental and theoretical study of the effects of a strong magnetic field applied perpendicular to a semiconductor quantum-well microcavity. The fundamental result is that the magnetic field increases the exciton-polariton splitting and time-resolved oscillation frequency by enhancing the exciton oscillator strength. The vacuum Rabi splitting is presented in direct relation to the quantum-well absorption at different magnetic-field strengths, which allows direct experimental verification of the square-root dependence of the splitting on oscillator strength. The oscillator strength enhancement is so pronounced, in fact, that we observe cavity mode couplings to light-hole-exciton transitions in high magnetic fields that are not present in low fields. In other words, the magnetic field enhances these weakly allowed transitions to such an extent that it propels the system from the weak coupling regime into the strong coupling regime.⁷ In our theoretical model, we first compute the magnetic-field-dependent exciton oscillator strength using a variational calculation which accounts for the field-induced shrinkage of the exciton envelope wave functions. The calculated oscillator strength is then inserted into a transfer matrix calculation, which yields the theoretical microcavity reflectance spectra. The predicted anticrossing curves and vacuum Rabi splittings are then obtained from the reflection dip energies. The theoretical calculations are in

excellent agreement with the data.

This paper is organized as follows. Section II describes the molecular-beam-epitaxy (MBE)-grown quantum-well microcavity structure and the experimental setup for measuring linear absorption and reflection spectra and the time-resolved vacuum-field Rabi oscillations under an applied magnetic field. Our experimental results and comparison with the theoretical model are discussed in Sec. III. We present the magnetic-field-dependent reflectance spectra, vacuum Rabi oscillations and splittings, and anticrossing curves in relation to the magnetoexciton oscillator strength computed directly from the measured quantum-well absorption. Finally, Sec. IV is a conclusion and outlook.

II. MICROCAVITY STRUCTURE AND EXPERIMENTAL SETUP

The quantum-well microcavity was grown by molecular-beam epitaxy on a GaAs substrate. The symmetric 99.5% reflectivity mirrors consist of 14- and 16.5-period Bragg reflectors made of alternating GaAs and AlAs quarter wave layers. A $3\lambda/2$ GaAs spacer was grown between the mirror stacks, and two 80 Å $\text{In}_{0.03}\text{Ga}_{0.97}\text{As}$ quantum wells were placed equally spaced from the cavity center to be at the antinodes of the intracavity field. At the sample's growth center, the cavity resonance frequency was designed to be below the exciton band edge, so that tuning of the cavity mode could be achieved by moving radially outward across the sample. In other words, the cavity mode energy increases monotonically with radial distance. The exciton shift with sample position is comparatively negligible for this quantum-well thickness. Hence by moving across the sample, the cavity mode can be brought into resonance with the electron $1s$ heavy-hole ($1s\text{HH}$) exciton transition, the electron $1s$ light-hole ($1s\text{LH}$) exciton transition, or, in the presence of strong magnetic field, with higher exciton transitions.

Quantum-well absorption spectra were measured using a white light probe beam transmitted through a 46 μm core diameter fiber that was placed directly on the front of the sample. Transmission was measured through the GaAs substrate. The microcavity reflectivity measurements were done by focusing the probe beam directly onto the sample with a 50 μm spot size. The vacuum-field Rabi oscillations were measured using a normally incident beam consisting of 150 fs pulses from a mode-locked Ti:sapphire laser with 82 MHz repetition rate. Light reflected from the microcavity was also collected at normal incidence and time resolved by a standard optical χ^2 frequency upconversion technique²¹ using a BBO (beta barium borate) crystal and a photomultiplier tube (PMT) with lock-in amplifier for detection. The samples were held at 1.6 K in the center of a liquid-helium-cooled superconducting magnet.

III. RESULTS AND DISCUSSION

A. Linear absorption as a function of magnetic field

Absorption spectra of 20 of the $\text{In}_{0.03}\text{Ga}_{0.97}\text{As}$ quantum wells are shown in Fig. 1 for increasing magnetic-field strengths. These spectra were measured using unpolarized light. The zero-field spectrum shows the $1s\text{HH1}$ exciton absorption peak at 1.486 eV, the continuum band edge at 1.492

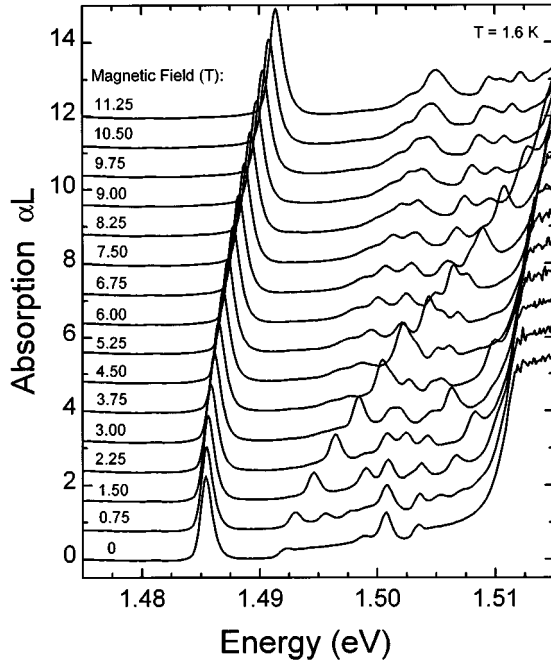


FIG. 1. Quantum-well absorption spectra for increasing magnetic-field strengths, using unpolarized light. The curves are vertically offset by 0.8.

eV, and the $1sLH1$ exciton at 1.501 eV. Although the quantum-well indium concentration was only 3%, the strain was sufficient to separate the $1sHH1$ and $1sLH1$ exciton transitions by 15 meV. With increasing magnetic-field strength, the continuum is quantized into a series of discrete Landau levels, and we see multiple absorption peaks emerge from the zero-field continuum. Also clearly observable is a diamagnetic shift of the exciton to higher energies. The $1s$ exciton transitions shift weakly with field, while the higher transitions shift more strongly. We compute the integrated absorption probability of the various exciton states as a measure of oscillator strength:^{18,19} $f_e \propto \int P_\alpha(E) dE$, where the integral is over the exciton linewidth and P_α is the absorption probability for one quantum well, $P_\alpha = 1 - e^{-\alpha L/N}$, N being the number of quantum wells. From this calculation, we find that f_e increases by a factor of 1.64 from zero to 11.25 T. This increase is manifested not only as an increase in the peak absorption, but also as an increase in the exciton linewidth. The oscillator strength enhancement is a result of the field-induced shrinkage of the exciton relative motion wave function, which enhances the electron-hole overlap. Wave-function shrinkage in real space corresponds to an expansion in k space, resulting in more available collision states. Hence the oscillator strength increase is manifested not only as an increase in the peak absorption, but also as a broadening of the exciton linewidth. Note that the broadening is larger than the Zeeman splitting, as will be shown below.

B. Quantum-well microcavity reflectance spectra

Figure 2 shows a series of reflectance spectra as the cavity field mode is tuned through resonance. On resonance, the strong coupling between the exciton and cavity modes results in a vacuum Rabi splitting of 4.53 meV. Note that the

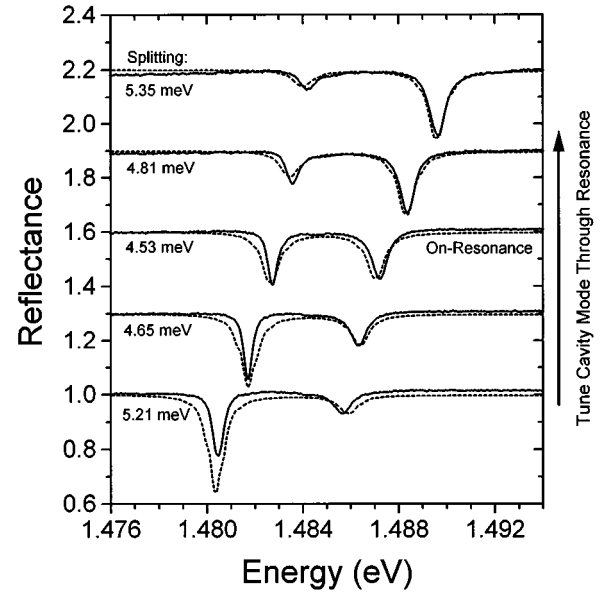


FIG. 2. Measured (solid lines) and calculated (dashed lines) reflectance spectra of the quantum-well microcavity in zero magnetic field as the cavity mode is tuned through the exciton resonance. The curves are vertically offset by 0.3.

splitting is small compared to the 15 meV separation between the $1sHH1$ and $1sLH1$ exciton transitions, permitting well-isolated lines. The low-energy peak has a full width at half maximum (FWHM) linewidth of 0.5 meV, while the high-energy peak has a linewidth of 0.8 meV. We attribute the linewidth asymmetry to the influence of the continuum absorption on the high-energy side. The minimum splitting to linewidth ratio is, to our knowledge, the largest value reported so far, and attests to the excellent sample quality.

C. Theoretical model

The theoretically calculated reflectance spectra are shown by the dashed lines in Fig. 2. We used an approach developed in Ref. 22, which is based on the exact solution of Maxwell's equations in the structure by a transfer matrix method²³ used in conjunction with a nonlocal dielectric response theory. This theory provides exact solutions for the reflectance spectra in the linear regime. The exciton oscillator strength is obtained through a variational calculation (see below). In the model, the change in the microcavity spacer length governs the energy detuning between photon and exciton modes.

In the basis of electric- and magnetic-field amplitudes the transfer matrix across a quantum well at normal incidence has a simple form:

$$\hat{T}_{\text{QW}} = \begin{bmatrix} 1 & 0 \\ -i2n_B\Gamma_0 & 1 \end{bmatrix}, \quad (1)$$

where n_B is the background refractive index in the barriers, ω_0 is the exciton resonance frequency, and Γ is the nonradiative damping rate. When the light frequency is sufficiently far from the resonance frequency of the medium, which is

the case for light propagation in Bragg mirrors, the transfer matrix across the j th layer has the form²⁴

$$\hat{T}_j = \begin{bmatrix} \cos\left(\frac{\omega}{c}n_j l_j\right) & -i\frac{1}{n_j}\sin\left(\frac{\omega}{c}n_j l_j\right) \\ -in_j\sin\left(\frac{\omega}{c}n_j l_j\right) & \cos\left(\frac{\omega}{c}n_j l_j\right) \end{bmatrix}, \quad (2)$$

where n_j and l_j are corresponding refractive indices and layer thicknesses. Knowing the transfer matrix of each layer, the matrix product $\hat{T} = \hat{T}_1 \hat{T}_2 \cdots \hat{T}_j \cdots \hat{T}_N$ gives the transfer matrix of the total system containing N layers. The reflection coefficient of the structure can be expressed via the elements of matrix \hat{T} as

$$R = \left| \frac{t_{11} + t_{12} - (t_{21} + t_{22}n_s)}{t_{11} + t_{12}n_s + t_{21} + t_{22}n_s} \right|^2, \quad (3)$$

where n_s is the refractive index of the substrate. In order to calculate the cavity spectrum, we have to determine three excitonic characteristics, namely, the resonance frequency and the nonradiative and radiative damping rates. In our case, ω_0 and Γ can be obtained from the spectra of Fig. 1 as the energy position and half-width of the corresponding exciton peak. We calculate Γ_0 from first principles by a variational solution of the magnetoexciton problem in a quantum well. The radiative damping rate is given by²⁰

$$\Gamma_0 = \frac{\omega_0}{c} n_B \frac{a_B^3}{a_{\perp}^2} I_{e,h}^2 \omega_{\text{LT}}^{\text{bulk}}, \quad (4)$$

where a_B and $\omega_{\text{LT}}^{\text{bulk}}$ are the exciton Bohr radius and longitudinal-transverse splitting in bulk GaAs (we used $a_B = 140 \text{ \AA}$ and $\hbar \omega_{\text{LT}}^{\text{bulk}} = 0.08 \text{ meV}$), and a_{\perp} and $I_{e,h}$ are the magnetic-field-dependent in-plane exciton Bohr radius and overlap integral of electron and hole envelopes, respectively. They are found by a self-consistent variational calculation described in detail in Ref. 25. The main point is that we fully take into account the ‘‘Coulomb well’’ effect, i.e., additional hole confinement in the adiabatic Coulomb potential created by electrons normal to the plane direction, which is of great importance in the vicinity of the type I–type II transition. Valence band offset values used in the calculation were calculated from the Bir and Pikus Hamiltonian.²⁶ We obtained the heavy-hole band offset $V_{\text{HH}} = 30 \text{ meV}$, and the light-hole band offset $V_{\text{LH}} = -3 \text{ meV}$, so that the band offset is type I for a heavy hole and type II for a light hole.

Additional complications arise in systems with type I–type II transitions, where there is no direct way to calculate the heavy- and light-hole effective masses, and, in general, the effective mass method is of limited utility since heavy-light hole mixing results in great nonparabolicity. We have obtained the best agreement between theoretical and experimental values of Γ_0 with normal-to-the-plane heavy- and light-hole masses $m_{\text{HH}} = 0.45m_0$, $m_{\text{LH}} = 0.15m_0$, and in-plane masses $m_{\text{HH}} = 0.35m_0$, $m_{\text{LH}} = 0.40m_0$, which are not far from the values predicted by the Luttinger Hamiltonian in the simplest diagonal approximation.

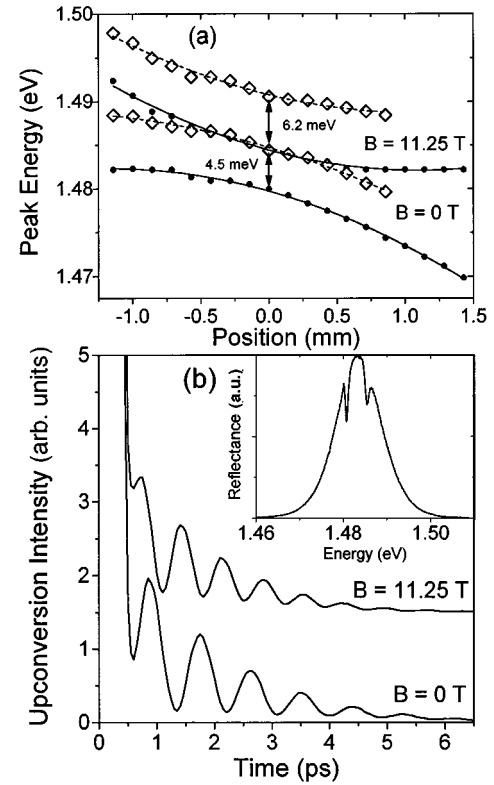


FIG. 3. (a) Anticrossing diagram, showing exciton-polariton peak energies vs detuning position. The lines are a guide to the eye. (b) Time-resolved vacuum field Rabi oscillations at $B = 0 \text{ T}$ (lower curve) and $B = 11.25 \text{ T}$ (upper curve, vertically offset by 1.5). The data are normalized to the reflected pump peak intensity at time zero and magnified by 1000. The inset shows the time-averaged reflected pulse spectrum at $B = 0 \text{ T}$.

D. Heavy-hole exciton/microcavity anticrossings and Rabi oscillations

Anticrossing curves for the $1s\text{HH1}$ exciton coupled to the cavity mode are shown in Fig. 3(a) for zero field (circles) and 11.25 T (diamonds). At zero detuning, the high-field peak energies are larger than the zero-field values due to the diamagnetic shift of the exciton. On resonance, $\hbar\Omega_0$ increases from 4.53 meV at zero field to 6.18 meV at 11.25 T. The time-resolved vacuum-field Rabi oscillations of Fig. 3(b) corroborate the cw data. The oscillation period at zero field is 0.89 ps in accordance with the 4.6 meV splitting observed in the reflected pulse spectrum shown in the inset. We observe a factor of 1.24 increase in the Rabi oscillation frequency at $B = 11.25 \text{ T}$, close to that expected from the measured oscillator strength increase and the cw results. The oscillations show a record depth of modulation due to the high sample quality, and decay exponentially at a rate characterized by spontaneous emission and cavity loss rates.

E. Magnetic-field dependence of oscillator strength and vacuum Rabi coupling

Figure 4 shows the relationship between exciton oscillator strength and normal-mode splitting. The relative oscillator strength $f_e(B)/f_e(0)$ is plotted versus magnetic field strength B in Fig. 4(a). The solid line shows the results of the

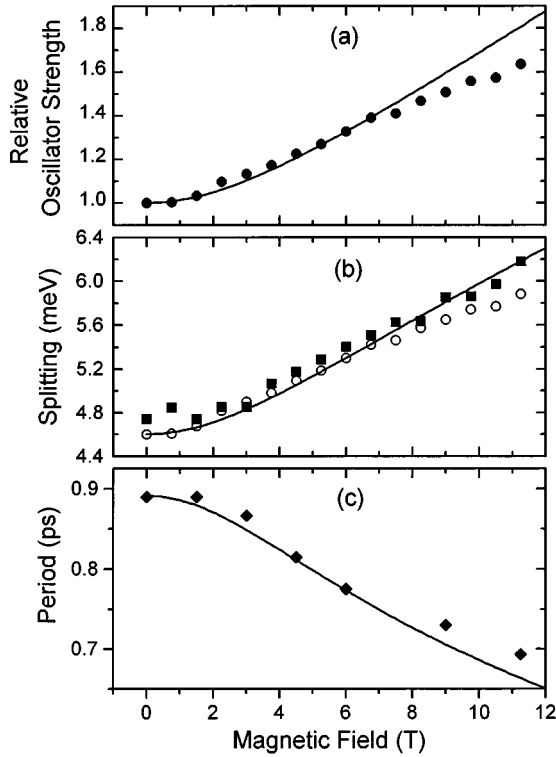


FIG. 4. (a) Relative oscillator strength of the $1sHH1$ exciton transition vs magnetic field. The circles represent measured values computed from integrating the $1sHH1$ absorption peaks of Fig. 1, while the solid line is the theoretical prediction based on the variational calculation. (b) Vacuum Rabi splitting vs magnetic field, showing measured values (squares), expected values calculated from the data points of (a) (open circles), and the theoretical prediction (solid line). (c) Measured Rabi oscillation period vs magnetic field (diamonds) and theory (solid line).

variational calculation described above,^{22,25} which takes into account the shrinkage of the in-plane electron-hole relative motion wave function under magnetic confinement. One can see reasonable agreement between theory and experiment. At low field strengths, we see almost no increase in f_e from 0 to 0.75 T. This is because the exciton wave function is perturbed very little at low fields, where the Coulomb interaction between electrons and holes is dominant over the magnetic field quantization. When the cyclotron energy of electron-hole pairs, $\hbar\omega_c = e\hbar B/\mu$, where μ is the reduced mass, becomes larger than the exciton binding energy, we begin to see an increase in f_e with increasing magnetic field. The deviation of the theoretical curve from the data at high fields can be attributed to some uncertainty in the heavy-hole in-plane mass, which is subjected to strong heavy-hole-light-hole mixing and strain effects. The exciton radiative damping obtained from the variational calculation is $\hbar\Gamma_0 = 0.04$ meV at zero field, which corresponds to $\hbar\Omega_0(0) = 4.6$ meV. Here we have doubled the oscillator strength in the calculation of Ω_0 to account for the two quantum wells in our microcavity.

Figure 4(b) shows the on-resonance splitting as a function of magnetic field. At each field strength, resonance was determined by choosing the position with the most symmetric reflectivity minima. Note that this criterion results in some error in obtaining the actual minimum splitting due to the

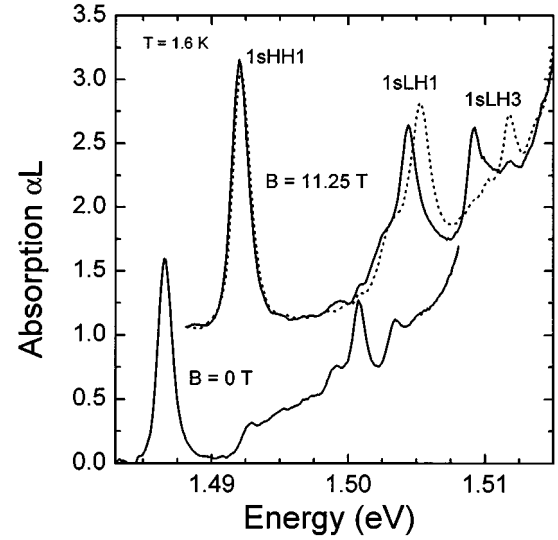


FIG. 5. Quantum-well absorption spectra in $B=0$ T (lower curve) and $B=11.25$ T (upper curves) for σ_+ (solid line) and σ_- (dotted line) circularly polarized light. The upper curves are vertically offset by 1.

influence of the continuum absorption. From the square-root dependence of the splitting on exciton oscillator strength, we have the relationship $\Omega_0(B) = \Omega_0(0)\sqrt{f_e(B)/f_e(0)}$. Taking the calculated first value $\hbar\Omega_0(0) = 4.6$ meV, the open circles show the expected result from the experimentally measured function $f_e(B)/f_e(0)$ [Fig. 4(a)], while the solid line comes from the theoretical dependence in Fig. 4(a). Linear dispersion theory²⁷ for an atomic transition of peak absorption coefficient α and linewidth δ gives $\Omega_0 \propto \sqrt{\alpha\delta}$, which is consistent with $\Omega_0 \propto \sqrt{\int \alpha(E)dE}$ here.

The time-resolved vacuum-field Rabi oscillation period vs magnetic field is plotted in Fig. 4(c). The data agree well with the theory (solid line), taken from the theoretical prediction of Fig. 4(b), calculating the oscillation period as $\tau = 2\pi/\Omega_0$.

F. Light-hole exciton vacuum-Rabi coupling

Until now we have considered only coupling of the cavity mode to the $1sHH1$ exciton transition. As shown in the absorption spectra of Fig. 1, energy level quantization by the magnetic field provides a large number of quantized states over which the cavity mode can be tuned. We can, in fact, tune the cavity mode over a series of excited transitions attributed to both heavy-hole and light-hole excitons. To identify these levels in the presence of a strong magnetic field, we first measured the absorption spectrum using a circularly polarized probe beam. Figure 5 shows the quantum-well absorption spectrum in zero field (lower curve) and in 11.25 T (upper curves) for σ_+ (solid line) and σ_- (dotted line) circularly polarized light. The polarizations σ_+ and σ_- are with respect to the magnetic-field vector. There is no difference in the zero-field absorption spectra for different polarizations. The spectra show, from left to right, the $1sHH1$ exciton transition, the $1sLH1$ exciton transition, and a third peak, identified as the $1sLH3$ exciton transition, where LH3 refers to the light-hole energy subband with quantum number $n=3$. We propose that the $1sLH3$ transition is weakly al-

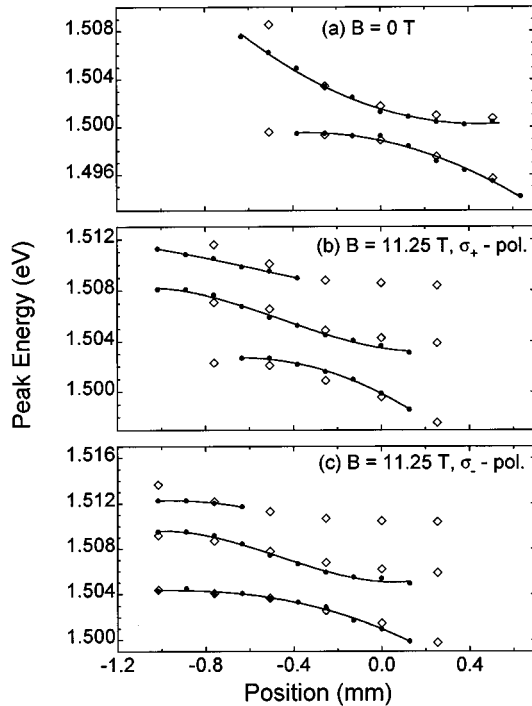


FIG. 6. Anticrossing diagrams, showing the cavity mode tuned through (a) $1sLH1$ exciton resonance in $B = 0$ T, and (b) and (c) $1sLH1$ and $1sLH3$ exciton resonances in $B = 11.25$ T, for (b) σ_+ and (c) σ_- circularly polarized light. Measured values (circles) and calculated values (diamonds) are in good agreement. The lines are a guide to the eye.

lowed in our $\text{In}_x\text{Ga}_{1-x}\text{As}$ quantum wells due to the very flat valence band, which enhances the overlap between electron and hole wave functions with different quantum numbers.²⁵ The $1sLH3$ exciton oscillator strength is very weak at zero field, but becomes significantly enhanced under magnetic confinement. In 11.25 T, the $1sHH1$ exciton exhibits a Zeeman splitting of only 0.1 meV, while the $1sLH1$ exciton splits by 0.86 meV, and the $1sLH3$ exciton by 2.6 meV.

Tuning of the cavity mode across the $1sLH1$ and $1sLH3$ excitons is shown in the anticrossing curves of Fig. 6. The data are plotted as circles, while the theoretical values (see below) are displayed as diamonds. The corresponding $1sLH1$ and $1sLH3$ exciton radiative dampings $\hbar\Gamma_0$ calculated by the variational method are plotted in Fig. 7 as a function of magnetic field. Figure 6(a) shows the anticrossing curve at zero magnetic field when the cavity is tuned to the $1sLH1$ exciton at 1.505 eV, with a minimum splitting of about 2 meV at zero detuning. This is roughly half the measured splitting for coupling to the $1sHH1$ exciton. Accordingly, we measure $f_{e,1sHH1}/f_{e,1sLH1} \approx 4$, from the integrated absorption spectra of Fig. 5. In this calculation, we subtracted the background absorption due to the GaAs substrate. Note that there is no apparent coupling to the $1sLH3$ exciton at zero field, which is explained by its small oscillator strength, as seen from the weak absorption line in the spectrum of Fig. 5. Indeed, Fig. 7 shows that the $1sLH3$ exciton oscillator strength is only half the $1sLH1$ value at zero field. In this case the criterion for strong coupling¹⁷ between the $1sLH3$ exciton and the cavity mode is not satisfied, so that no polariton splitting is observed.

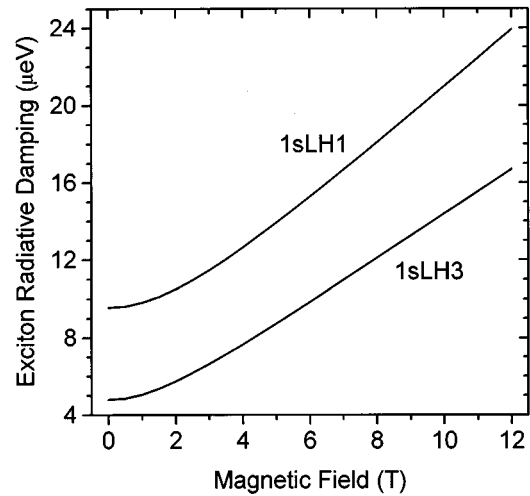


FIG. 7. $1sLH1$ (top curve) and $1sLH3$ (bottom curve) exciton radiative dampings $\hbar\Gamma_0$ vs magnetic field calculated using the variational method.

This is no longer the case in $B = 11.25$ T, where the $1sLH3$ transition becomes strongly coupled to the cavity mode. Figures 6(b) and 6(c) show anticrossing curves in $B = 11.25$ T for σ_+ and σ_- circularly polarized light, respectively. As the cavity is tuned to higher energies, it becomes strongly coupled first to the $1sLH1$ exciton at 1.505 eV, and then to the $1sLH3$ exciton at 1.510 eV. Note the qualitative change in the shape of the anticrossing curves from the zero-field case. After the cavity mode is tuned across the $1sLH1$ exciton, it then begins to couple to the next available state, the $1sLH3$ exciton, and changes its course significantly. As one can see from Fig. 7, in $B = 11.25$ T, the oscillator strength for the $1sLH3$ transition is increased by a factor of 3 compared to the zero-field value. The strong coupling regime is definitely reached with the magnetic-field increase.

The observed double anticrossings result from coupling between two exciton resonances via the photon mode. In this case, the direct comparison of polariton splittings with the measured and calculated oscillator strengths has no meaning. The shape of the anticrossing curves, however, is still governed by the oscillator strengths of the participating exciton transitions. The diamonds in Fig. 6 show the energies of the dips in the theoretical reflectance spectra, calculated by the transfer matrix method. The radiative damping rates have been taken from Fig. 7. Tuning of the photon mode across the exciton resonances was achieved by varying the micro-cavity spacer length in the model structure. Thus we tuned the bare optical mode in the model from 1.496 eV to 1.508 eV in Fig. 6(a), from 1.497 eV to 1.511 eV in Fig. 6(b), and from 1.500 eV to 1.514 eV in Fig. 6(c). For comparison between theory and experiment in Fig. 6 it has been assumed that the spacer length depends linearly on the position at the sample, which is a reasonable approximation over this small tuning range. One can see that the single anticrossing in zero field and the double anticrossings in 11.25 T are well reproduced by the theory. The theoretical splittings do, however, exceed the experimental ones at certain positions, which probably indicates the limited accuracy of the one-parameter variational theory in this case. Note that the different forms of the double anticrossings for σ_+ and σ_- polarizations are

connected with different splittings between the $1sLH1$ and $1sLH3$ excitons caused by different hole g factors.²⁸ Three-oscillator coupling has also been observed in semiconductor microcavities with two different quantum wells, where the heavy-hole excitons from the two quantum wells are coupled via the photon mode.²⁹ The double anticrossings presented here nicely demonstrate how the magnetic confinement brings the $1sLH3$ transition into the strong coupling regime, leading to a three-oscillator coupling that is not observed at low fields.

IV. CONCLUSION

This paper has investigated magnetic-field effects on vacuum Rabi coupling in a semiconductor quantum-well microcavity. We have shown that the magnetic field enhances the exciton oscillator strength, as experimentally observed from the integrated quantum-well absorption spectra. This enhanced oscillator strength then results in an increase in the vacuum Rabi splitting and corresponding oscillation frequency between exciton and cavity modes. The coupling strength increase was shown to be so pronounced that the

magnetic-field propels weak exciton transitions into the strong coupling regime. This phenomenon was observed as three-oscillator coupling in strong magnetic fields, where only two-oscillator coupling was observed in zero field. Note that all of the results presented here were measured in the linear regime. In order to fully elucidate strong confinement effects on the vacuum Rabi coupling in semiconductor microcavities, magnetic field-dependent studies must continue into the nonlinear regime, where exciton bleaching^{30,31} and broadening³² become important.

ACKNOWLEDGMENTS

This work was supported in part by the National Science Foundation's Lightwave Technology and Physics divisions, by the Joint Services Optics Program (Air Force Office of Scientific Research and Army Research Office), by the Advanced Research Projects Agency's Ultra Photonics division, and by COEDIP. It is a pleasure to thank S. V. Goupalov for help with the numerical calculations, and H. Giessen, P. Meystre, and R. P. Seisyan for their critical reading of the manuscript.

-
- ¹For recent reviews of cavity QED see, e.g., *Spontaneous Emission and Laser Oscillation in Microcavities*, edited by H. Yokoyama and K. Ujihara (CRC Press, Boca Raton, FL, 1995); *Cavity Quantum Electrodynamics*, edited by P.R. Berman (Academic, Boston, 1994); S. Haroche, in *Fundamental Systems in Quantum Optics*, edited by J. Dalibard, J.-M. Raimond, and J. Zinn-Justin (North-Holland, Amsterdam, 1992).
- ²*Confined Electrons and Photons: New Physics and Devices*, edited by E. Burstein and C. Weisbuch (Plenum, New York, 1994).
- ³Here we use "strong coupling" to describe the case in which $\Omega_0 = \sqrt{N}g \gg \kappa, \gamma$, where N is the number of emitters and g is the dipole coupling strength for a single emitter. A more stringent criterion requires $g \gg \kappa, \gamma$, i.e., strong coupling for a single emitter.
- ⁴O. Akimoto and H. Hasegawa, *J. Phys. Soc. Jpn.* **22**, 181 (1967).
- ⁵M. Shinada and K. Tanaka, *J. Phys. Soc. Jpn.* **29**, 1258 (1970).
- ⁶S. Schmitt-Rink, J.B. Stark, W.H. Knox, D.S. Chemla, and W. Schäfer, *Appl. Phys. A* **53**, 491 (1991).
- ⁷J. Tignon, P. Voisin, C. Delalande, M. Voos, R. Houdré, U. Oesterle, and R.P. Stanley, *Phys. Rev. Lett.* **74**, 3967 (1995).
- ⁸T.A. Fisher, A.M. Afshar, P. Kinsler, D.M. Whittaker, M.S. Skolnick, J.S. Roberts, G. Hill, and M.A. Pate (unpublished).
- ⁹J.J. Hopfield, *Phys. Rev.* **112**, 1555 (1958).
- ¹⁰C. Weisbuch, M. Nishioka, A. Ishikawa, and Y. Arakawa, *Phys. Rev. Lett.* **69**, 3314 (1992).
- ¹¹R. Houdré, R.P. Stanley, U. Oesterle, M. Ilegems, and C. Weisbuch, *Phys. Rev. B* **49**, 16 761 (1994).
- ¹²See, e.g., H. Haug and S.W. Koch, in *Quantum Theory of the Optical and Electronic Properties of Semiconductors* (World Scientific, Singapore, 1990).
- ¹³T.B. Norris, J.-K. Rhee, C.-Y. Sung, Y. Arakawa, M. Nishioka, and C. Weisbuch, *Phys. Rev. B* **50**, 14 663 (1994).
- ¹⁴H. Cao, J. Jacobson, G. Björk, S. Pau, and Y. Yamamoto, *Appl. Phys. Lett.* **66**, 1107 (1995).
- ¹⁵J. Jacobson, S. Pau, H. Cao, G. Björk, and Y. Yamamoto, *Phys. Rev. A* **51**, 2452 (1995).
- ¹⁶H. Wang, J. Shah, T.C. Damen, L.N. Pfeiffer, and J.E. Cunningham, *Phys. Status Solidi B* **188**, 381 (1995).
- ¹⁷V. Savona, L.C. Andreani, P. Schwendimann, and A. Quattropani, *Solid State Commun.* **93**, 733 (1995).
- ¹⁸M. Sugawara, *Phys. Rev. B* **45**, 11 423 (1992).
- ¹⁹M. Sugawara, N. Okazaki, T. Fujii, and S. Yamazaki, *Phys. Rev. B* **48**, 8848 (1993).
- ²⁰A.V. Kavokin, A.I. Nesvizhskii, and R.P. Seisyan, *Semiconductors* **27**, 530 (1993).
- ²¹J. Shah, *IEEE J. Quantum Electron.* **QE-24**, 276 (1988).
- ²²A.V. Kavokin and M.A. Kaliteevski, *Solid State Commun.* **95**, 859 (1995).
- ²³H.A. MacLeod, *Thin Film Optical Filters* (Hilger, Bristol, 1986).
- ²⁴M. Born and E. Wolf, *Principles of Optics* (Pergamon, Oxford, 1980).
- ²⁵R.P. Seisyan, A.V. Kavokin, S.I. Kokhanovskii, A.I. Nesvizhskii, M.E. Sasin, M.A. Sinitzin, and B.S. Yavich, *Semicond. Sci. Technol.* **10**, 611 (1995).
- ²⁶G.L. Bir and G.E. Pikus, *Symmetry and Strain-Induced Effects in Semiconductors* (Wiley, New York, 1974).
- ²⁷Y. Zhu, D.J. Gauthier, S.E. Morin, Q. Wu, H.J. Carmichael, and T.W. Mossberg, *Phys. Rev. Lett.* **64**, 2499 (1990).
- ²⁸E.L. Ivchenko and A.A. Kiselev, *Sov. Phys. Semicond.* **26**, 827 (1992).
- ²⁹E.K. Lindmark, T.R. Nelson, Jr., G. Khitrova, H.M. Gibbs, A.V. Kavokin, and M.A. Kaliteevski (unpublished).
- ³⁰J.-K. Rhee, R. Lai, T.B. Norris, Y. Arakawa, and M. Nishioka, *Technical Digest Series Conference Edition* (Optical Society of America, Washington, D.C., 1995), Vol. 16. pp. 226 and 227.
- ³¹R. Houdré, J.L. Gibernon, P. Pellandini, R.P. Stanley, U. Oesterle, C. Weisbuch, J. O'Gorman, B. Roycroft, and M. Ilegems, *Phys. Rev. B* **52**, 7810 (1995).
- ³²G. Khitrova, K. Tai, E.K. Lindmark, T.R. Nelson, Jr., D.V. Wick, J.D. Berger, O. Lyngnes, J. Prineas, S. Park, H.M. Gibbs, and Y. Lai (unpublished).